




Cite this: DOI: 10.1039/d0tc01054e

Blue-green-emitting cationic iridium complexes with oxadiazole-type counter-anions and their use for highly efficient solution-processed organic light-emitting diodes†

Xianwen Meng, Pei Wang, Rubing Bai and Lei He *

Cationic iridium complexes are promising phosphorescent dopants for solution-processed organic light-emitting diodes (OLEDs) and counter-anion control has emerged as a facile approach to tailor their properties for high-performance devices. A series of oxadiazole-type anions, 3-(5-phenyl-1,3,4-oxadiazol-2-yl)benzenesulfonate (OXD-SO_3^-), 3-(5-(4-(*tert*-butyl)phenyl)-1,3,4-oxadiazol-2-yl)benzenesulfonate (tBuOXD-SO_3^-) and 3-(5-(4-(*tert*-butyl)phenyl)-1,3,4-oxadiazol-2-yl)phenyltrifluoroborate (tBuOXD-BF_3^-), have been prepared as counter-anions for blue-green-emitting cationic iridium complexes. The photophysical and electrochemical properties of the anions and the complexes have been comprehensively characterized. The anions do not affect the emission properties of the phosphorescent cation and efficiently transfer their energy to the cations in films. Solution-processed, double-layer OLEDs using the complexes as dopants have shown much higher ($\times 1.4$) efficiencies than the device using the reference complex with a PF_6^- counter-anion, owing to the improvement of carrier transport/recombination balance by the electron-trapping effect of oxadiazole-type anions. In particular, the blue-green device using the complex with the OXD-SO_3^- counter-anion affords a peak current efficiency of 37.6 cd A^{-1} and a peak external quantum efficiency (EQE) of 15.2%, which is the highest for solution-processed OLEDs based on cationic iridium complexes reported so far.

Received 1st March 2020,
Accepted 31st March 2020

DOI: 10.1039/d0tc01054e

rsc.li/materials-c

1. Introduction

Organic light-emitting diodes (OLEDs) have emerged as promising thin-film emissive devices for lighting or display applications.^{1,2} Because OLEDs are composed of multiple carrier-injecting/transporting and emitting layers sandwiched between two electrodes, thin-film deposition technology plays a key role in the fabrication of OLEDs. Most OLEDs are made by depositing the organic layers through thermal evaporation under high vacuum, which is cost-inefficient and unfriendly for mass production.² OLEDs can also be fabricated by solution-processing technologies such as inkjet printing, spray coating and slot-die coating, which do not require high-vacuum condition and thus significantly reduce the production cost.^{2,3} For this notable advantage, solution-processed OLEDs have experienced a rapid development in the past decades.^{2,4–11}

In recent years, cationic iridium complexes have emerged as promising phosphorescent dopants for solution-processed OLEDs, because of their capability to afford an internal quantum

efficiency of up to 100% for devices, facile tuning on emission properties, and good solubility in polar solvent.^{12–33} In general, cationic iridium complexes have a form of $[\text{Ir}(\text{C}^{\wedge}\text{N})_2(\text{N}^{\wedge}\text{N})]^+\text{A}^-$, with $[\text{Ir}(\text{C}^{\wedge}\text{N})_2(\text{N}^{\wedge}\text{N})]^+$ as the phosphorescent cation and A^- as the counter anion ($\text{C}^{\wedge}\text{N}$ is the cyclometalating ligand and $\text{N}^{\wedge}\text{N}$ is the ancillary ligand).^{12,34,35} Previous researches have been focused on modifying $[\text{Ir}(\text{C}^{\wedge}\text{N})_2(\text{N}^{\wedge}\text{N})]^+$ through judicious ligand control to tune the phosphorescent properties,^{12–23,25,28–31,33} but the counter anion A^- , which is usually PF_6^- , has rarely been considered.^{24,27,32,36} When the complexes are used as active components in light-emitting devices, the small PF_6^- anions migrate within the layers under external electrical field, which is essential for the operation of light-emitting electrochemical cells (LECs)^{12,35,37} but is unwanted for the operation of OLEDs. Bulky anions such as tetraphenylborate and its derivatives have been used as counter-anions, which render the complexes with good volatility to enable the fabrication of vacuum-deposited OLEDs;^{12,36,38–42} in a special case, a small chlorine ion has been used as the counter-anion in a cationic iridium complex for vacuum-deposited OLED.⁴³ However, like PF_6^- , these anions are still optoelectronically inactive, which cannot largely enhance the performances of the complexes in OLEDs. So far, cationic iridium complexes have shown lower performances than neutral

College of Chemistry, Key Laboratory of Pesticide and Chemical Biology of Ministry of Education, Hubei International Scientific and Technological Cooperation Base of Pesticide and Green Synthesis, Central China Normal University, Wuhan 430079, People's Republic of China. E-mail: helei@mail.ccnu.edu.cn

† Electronic supplementary information (ESI) available. See DOI: 10.1039/d0tc01054e

iridium complexes in OLEDs,^{5,7,8} which leaves large space for further improvements. The lower device performances for cationic iridium complexes compared to the neutral counterparts can be ascribed to (i) unbalanced carrier-recombination and exciton leakage to adjacent layers in solution-processed OLEDs with simple device structure (usually double-layer structure), and (ii) lower luminescent efficiencies of cationic iridium complexes compared to well-studied neutral complexes, especially for blue-emitting ones.^{35,44} These issues need to be addressed by judicious molecular design and device engineering.

It is noted that $[\text{Ir}(\text{C}^{\wedge}\text{N})_2(\text{N}^{\wedge}\text{N})]^+$ and A^- are closely bound together by electrostatic interactions between them yet they can be independently varied. Rendering the counter-anions with optoelectronic properties represents a facile approach to tune the overall optoelectronic properties of the complexes.^{45,46} In this regard, carrier-trapping/transporting anions are promising counter-anions for cationic iridium complexes used in OLEDs, because they are bulky and immobile, and more importantly, can tune carrier transport/recombination balance in the emissive layers by carrier-trapping/transporting on the complexes.^{27,32} Here we report blue-green-emitting cationic iridium complexes with electron-deficient oxadiazole-type counter-anions and their use as dopants for highly efficient solution-processed OLEDs (Chart 1). 2,5-Diphenyl-1,3,4-oxadiazole (OXD) is used as the core of the anion because of its electron-deficiency for electron-trapping/transporting and high triplet energy (~ 2.7 eV) for confining triplet energy on the phosphorescent cation.^{47,48} 1,3,4-oxadiazole derivatives have previously been used as ancillary ligands in cationic iridium complexes.⁴⁹ In our work, SO_3^- or BF_3^- are anchored to OXD to afford three anions: 3-(5-phenyl-1,3,4-oxadiazol-2-yl)benzenesulfonate (OXD-SO_3^-), 3-(5-(4-(*tert*-butyl)phenyl)-1,3,4-oxadiazol-2-yl)benzenesulfonate ($t\text{BuOXD-SO}_3^-$) and 3-(5-(4-(*tert*-butyl)phenyl)-1,3,4-oxadiazol-2-yl)phenyltrifluoroborate ($t\text{BuOXD-BF}_3^-$). The photophysical and electrochemical properties of the anions and the complexes have been comprehensively investigated. The oxadiazole-type anions affect neither the emission color nor the efficiency of the phosphorescent cation. In films, efficient energy-transfer occur from the anions to the phosphorescent cation because of the close proximity between them.

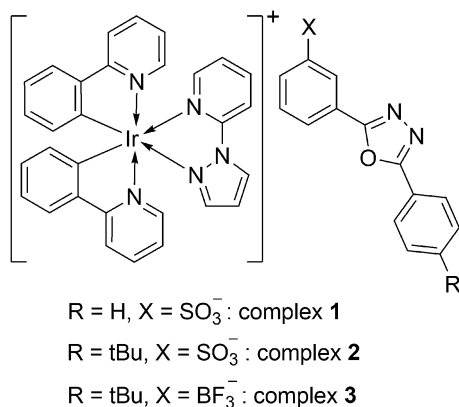


Chart 1 Chemical structures of cationic iridium complexes **1–3** with oxadiazole-type counter-anions. *t*Bu is short for *tert*-butyl.

Solution-processed, double-layer, blue-green OLEDs using complexes **1–3** afford much higher performances than the reference device using the complex with a PF_6^- counter-anion, with high peak current-efficiencies of up to 37.6 cd A^{-1} and external quantum efficiencies (EQEs) of up to 15.2%, which is the highest for solution-processed OLEDs using cationic iridium complexes as dopants reported so far (Table S1, ESI†),^{13–32} and even comparable to the highest one (EQE = 16.4% for a green-yellow device) reported for multilayer vacuum-evaporation OLEDs using cationic iridium complexes.⁴⁰ These efficiencies are also comparable to those afforded by solution-processed OLEDs using neutral iridium complexes.^{5,7}

2. Experimental

2.1. General information

A BRUKER 400/500 NMR spectrometer, a LTQ-ORBITRAP-ETD mass spectrometer and an EA3000 elemental analyzer were used for measurements of NMR spectra, mass spectrometry and elemental analysis, respectively. A Macy UV-1800 UV-vis spectrophotometer and a Gangdong F-320 fluorospectrophotometer were used to measure absorption and photoluminescence (PL) spectra, respectively. A transient spectrofluorometer equipped with an integrating sphere (Edinburgh Instruments, FLS1000) was used to measure PL transient lifetimes and photoluminescent efficiencies in thin films. The photoluminescent efficiencies in degassed CH_3CN solution were measured *versus* quinine sulfate ($\Phi_p = 0.545$ in 1 M H_2SO_4). A LK1100 voltammetric analyzer was used to conduct cyclic voltammetry in solution (10^{-3} M) at a scan rate of 100 mV s^{-1} , with a glass-carbon working electrode, a silver-wire pseudo-reference electrode and a platinum-wire counter electrode. The supporting electrolyte and the internal standard are tetrabutylammonium hexafluorophosphate (0.1 M) and ferrocene, respectively. The solutions were degassed with argon for cyclic voltammetry experiments.

2.2. Materials

Unless otherwise stated, all reactants and solvents were purchased from commercial sources and used as received. $[\text{Ir}(\text{ppy})_2(\text{pzpy})]^+\text{Cl}^-$ and $[\text{Ir}(\text{ppy})_2(\text{pzpy})]\text{PF}_6$ were prepared according to reported procedures.^{27,50}

Synthesis of sodium 3-(hydrazinecarbonyl)benzenesulfonate (1). Sodium 3-carboxybenzenesulfonate (4.0 g, 17.8 mmol) and concentrated HCl solution (1.5 mL, 18 mmol) were dissolved in ethanol (40 mL). The mixture was stirred at 70°C under a nitrogen atmosphere for 5 h to produce sodium 3-(ethoxycarbonyl)benzenesulfonate. To the solution, hydrazine hydrate (20 mL) were added dropwise. The solution was refluxed under a nitrogen atmosphere for 12 h. After being cooled to room temperature, the mixture was filtered. To the filtrate, sodium hydroxide (1.6 g, 40 mmol) dissolved in ethanol (15 mL) was added under stirring. The mixture was stirred at room temperature for 3 h. The precipitate was collected and dried under vacuum, affording the pure product as a white solid (3.6 g, 15 mmol). Yield: 84%. $^1\text{H-NMR}$ (500 MHz, $\text{DMSO}-d_6$, δ [ppm]): 9.78 (s, 1H), 8.08 (s, 1H),

7.79–6.69 (m, 2H), 7.36 (t, $J = 8$ Hz, 1H), 4.46 (s, 2H). HRMS (ESI, m/z): 215.01328 $[M - Na]^+$ (calc. 215.01320).

Synthesis of sodium 3-(2-benzylidenehydrazine-1-carbonyl)benzenesulfonate (2). Sodium 3-(hydrazinecarbonyl)benzenesulfonate (2.4 g, 10 mmol) and benzaldehyde (1.3 g, 12 mmol) were dissolved in ethanol (100 mL). The mixture was refluxed for 12 h and then cooled to room temperature. The precipitate was collected, affording the pure product as a white solid (2.1 g, 6.5 mmol). Yield: 65%. $^1\text{H-NMR}$ (500 MHz, $\text{DMSO-}d_6$, δ [ppm]): 12.09 (s, 1H), 8.55 (s, 1H), 8.22 (s, 1H), 7.93 (d, $J = 7.5$ Hz, 1H), 7.81 (d, $J = 7.5$ Hz, 1H), 7.74 (d, $J = 6.5$ Hz, 2H), 7.53–7.42 (m, 4H). HRMS (ESI, m/z): 303.04486 $[M - Na]^+$ (calc. 303.04450).

Synthesis of sodium 3-(2-(4-(*tert*-butyl)benzylidene)hydrazine-1-carbonyl)benzenesulfonate (3). The synthesis of compound 3 was similar to that of compound 2, except that 4-(*tert*-butyl)benzaldehyde replaced benzaldehyde. Yield: 65%. $^1\text{H-NMR}$ (500 MHz, $\text{DMSO-}d_6$, δ [ppm]): 11.94 (s, 1H), 8.48 (s, 1H), 8.20 (s, 1H), 7.88 (d, $J = 7.5$ Hz, 1H), 7.81 (d, $J = 7.5$ Hz, 1H), 7.67 (d, $J = 8.0$ Hz, 2H), 7.53–4.45 (m, 3H), 1.31 (s, 9H). HRMS (ESI, m/z): 359.10645 $[M - Na]^+$ (calc. 359.10710).

Synthesis of sodium 3-(5-phenyl-1,3,4-oxadiazol-2-yl)benzenesulfonate (OXD- SO_3Na). Sodium 3-(2-benzylidenehydrazine-1-carbonyl)benzenesulfonate (2.0 g, 6.0 mmol), iodine (2.2 g, 8.7 mmol) and K_2CO_3 (1.7 g, 12 mmol) were suspended in dry DMSO (10 mL). The mixture was stirred at 100 °C under a nitrogen atmosphere for 4 h. After being cooled to room temperature, sodium thiosulfate (1.1 g, 6.8 mmol) was added to the reaction mixture. The mixture was stirred at room temperature for 3 h and then brine solution was added. The precipitate was collected and purified by column chromatography on silica gel with $\text{CH}_2\text{Cl}_2/\text{CH}_3\text{OH}$ (5:1) as the eluent, affording the pure product as a white solid (1.6 g, 4.9 mmol). Yield: 82%. $^1\text{H-NMR}$ (500 MHz, $\text{DMSO-}d_6$, δ [ppm]): 8.34 (s, 1H), 8.15 (d, $J = 7.2$ Hz, 2H), 8.10 (d, $J = 7.5$ Hz, 1H), 7.87 (d, $J = 7.5$ Hz, 1H), 7.71–7.59 (m, 4H). $^{13}\text{C-NMR}$ (126 MHz, $\text{DMSO-}d_6$, δ [ppm]): 164.56, 164.36, 149.90, 132.52, 129.92, 129.59, 129.47, 127.20, 124.14, 123.82, 123.35. HRMS (ESI, m/z): 301.02881 $[M - Na]^+$ (calc. 301.02885).

Synthesis of sodium 3-(5-(4-(*tert*-butyl)phenyl)-1,3,4-oxadiazol-2-yl)benzenesulfonate (*t*BuOXD- SO_3Na). The synthesis of *t*BuOXD- SO_3Na was similar to that of OXD- SO_3Na , except that sodium 3-(2-(4-(*tert*-butyl)benzylidene)hydrazine-1-carbonyl)benzenesulfonate replaced sodium 3-(2-benzylidenehydrazine-1-carbonyl)benzenesulfonate. Yield: 84%. $^1\text{H-NMR}$ (500 MHz, $\text{DMSO-}d_6$, δ [ppm]): 8.31 (s, 1H), 8.12–8.03 (m, 3H), 7.85 (d, $J = 7.7$ Hz, 1H), 7.67 (d, $J = 8.4$ Hz, 2H), 7.61 (t, $J = 7.7$ Hz, 1H), 1.34 (s, 9H). $^{13}\text{C-NMR}$ (126 MHz, $\text{DMSO-}d_6$, δ [ppm]): 164.60, 164.19, 155.50, 150.01, 129.58, 129.41, 127.11, 127.08, 126.75, 124.08, 123.40, 121.13, 35.33, 31.31. HRMS (ESI, m/z): 357.08997 $[M - Na]^+$ (calc. 357.09145).

Synthesis of potassium (3-(5-(4-(*tert*-butyl)phenyl)-1,3,4-oxadiazol-2-yl)phenyl)trifluoroborate (*t*BuOXD- BF_3K). (3-(5-(4-(*tert*-butyl)phenyl)-1,3,4-oxadiazol-2-yl)phenyl)boronic acid (1.1 g, 3.5 mmol) was dissolved in methanol (100 mL). To the solution, KHF_2 (0.8 g, 10 mmol) dissolved in H_2O (10 mL) was added dropwise. The mixture was stirred at room temperature for 1 h and then concentrated and filtered. The precipitate was collected and dried under vacuum, affording a white solid (1.2 g, 3.1 mmol). Yield: 88%.

$^1\text{H-NMR}$ (500 MHz, $\text{DMSO-}d_6$, δ [ppm]): 8.10–8.01 (m, 3H), 7.83 (d, $J = 7.5$ Hz, 1H), 7.65 (d, $J = 7.8$ Hz, 2H), 7.58 (d, $J = 7.3$ Hz, 1H), 7.35 (t, $J = 7.5$ Hz, 1H), 1.34 (s, 9H). $^{13}\text{C-NMR}$ (126 MHz, $\text{DMSO-}d_6$, δ [ppm]): 165.60, 164.06, 155.21, 135.67, 130.05, 127.69, 126.89, 126.72, 124.10, 121.79, 121.39, 35.30, 31.33. HRMS (ESI, m/z): 345.13838 $[t\text{BuOXD-BF}_3]^+$ (calc. 345.13915).

Synthesis of $[\text{Ir}(\text{ppy})_2(\text{pzpy})]^+[\text{OXD-SO}_3^-]$ (complex 1). OXD- SO_3Na (130 mg, 0.4 mmol) was dissolved in methanol/deionized water (15/15 mL). To the solution, $[\text{Ir}(\text{ppy})_2(\text{pzpy})]^+\text{Cl}^-$ (272 mg, 0.4 mmol) dissolved in methanol/deionized water (15/15 mL) was added dropwise. The mixture was stirred at room temperature for 1 h and then concentrated. The precipitate was collected, recrystallized from $\text{CH}_3\text{OH}/\text{H}_2\text{O}$ and dried under vacuum at 80 °C, affording the pure product as a yellow powder (300 mg, 0.32 mmol). Yield: 80%. $^1\text{H-NMR}$ (500 MHz, $\text{DMSO-}d_6$, δ [ppm]): 9.31 (d, $J = 2.9$ Hz, 1H), 8.53 (d, $J = 8.5$ Hz, 1H), 8.37–8.30 (m, 2H), 8.30–8.24 (m, 2H), 8.15 (d, $J = 6.0$ Hz, 2H), 8.10 (d, $J = 7.7$ Hz, 1H), 7.97 (t, $J = 7.8$ Hz, 2H), 7.93–7.87 (m, 2H), 7.85 (d, $J = 7.7$ Hz, 1H), 7.77 (d, $J = 5.7$ Hz, 1H), 7.72 (d, $J = 5.6$ Hz, 1H), 7.69–7.57 (m, 5H), 7.54 (t, $J = 7.0$ Hz, 1H), 7.29 (s, 1H), 7.24 (t, $J = 6.6$ Hz, 1H), 7.20 (t, $J = 6.6$ Hz, 1H), 7.05–6.96 (m, 2H), 6.94–6.82 (m, 3H), 6.19 (t, $J = 7.9$ Hz, 2H). $^{13}\text{C-NMR}$ (126 MHz, $\text{DMSO-}d_6$, δ [ppm]): 167.32, 167.18, 164.56, 164.40, 150.10, 149.69, 149.62, 149.56, 149.19, 148.65, 146.59, 144.58, 144.53, 143.74, 142.23, 139.40, 139.27, 133.23, 132.51, 131.77, 131.60, 130.63, 130.20, 129.92, 129.56, 129.47, 127.21, 127.12, 125.78, 125.55, 125.19, 124.40, 124.27, 124.15, 123.85, 123.34, 122.85, 122.63, 120.46, 120.41, 114.05, 112.03. HRMS (ESI, m/z): 646.15574 $[\text{Ir}(\text{ppy})_2(\text{pzpy})]^+$ (calc. 646.15772); 301.02874 $[\text{OXD-SO}_3]^-$ (calc. 301.02885). Anal. found: C, 55.59; H, 3.63; N, 10.31. Anal. calcd for $\text{C}_{44}\text{H}_{32}\text{IrN}_7\text{O}_4\text{S}$: C, 55.80; H, 3.41; N, 10.35.

Synthesis of $[\text{Ir}(\text{ppy})_2(\text{pzpy})]^+[t\text{BuOXD-SO}_3^-]$ (complex 2). The synthesis of complex 2 followed a procedure similar to that for complex 1, except that *t*BuOXD- SO_3Na replaced OXD- SO_3Na . Yield: 82%. $^1\text{H-NMR}$ (500 MHz, $\text{DMSO-}d_6$, δ [ppm]): 9.31 (d, $J = 2.3$ Hz, 1H), 8.53 (d, $J = 8.5$ Hz, 1H), 8.38–8.30 (m, 2H), 8.27 (d, $J = 7.8$ Hz, 2H), 8.07 (d, $J = 7.6$ Hz, 3H), 7.97 (t, $J = 7.5$ Hz, 2H), 7.93–7.82 (m, 3H), 7.78–7.72 (m, 2H), 7.69–7.64 (m, 3H), 7.61 (t, $J = 7.7$ Hz, 1H), 7.54 (t, $J = 6.5$ Hz, 1H), 7.29 (s, 1H), 7.26–7.18 (m, 2H), 7.07–6.95 (m, 2H), 6.95–6.82 (m, 3H), 6.20 (t, $J = 8.0$ Hz, 2H), 1.34 (s, $J = 8.0$ Hz, 9H). $^{13}\text{C-NMR}$ (126 MHz, $\text{DMSO-}d_6$, δ [ppm]): 166.76, 166.62, 164.02, 163.64, 154.92, 149.55, 149.11, 149.04, 148.99, 148.62, 148.09, 146.01, 144.01, 143.96, 143.17, 141.66, 138.83, 138.69, 132.66, 131.20, 131.03, 130.05, 129.63, 128.98, 128.84, 126.51, 126.17, 125.21, 124.98, 124.62, 123.82, 123.69, 123.52, 122.82, 122.27, 122.05, 120.57, 119.89, 119.83, 113.48, 111.46, 34.76, 30.74. HRMS (ESI, m/z): 646.15521 $[\text{Ir}(\text{ppy})_2(\text{pzpy})]^+$ (calc. 646.15772); 357.09064 $[t\text{BuOXD-SO}_3]^-$ (calc. 357.09145). Anal. found: C, 57.24; H, 4.28; N, 9.65. Anal. calcd for $\text{C}_{48}\text{H}_{40}\text{IrN}_7\text{O}_4\text{S}$: C, 57.47; H, 4.02; N, 9.77.

Synthesis of $[\text{Ir}(\text{ppy})_2(\text{pzpy})]^+[t\text{BuOXD-BF}_3^-]$ (complex 3). The synthesis of complex 3 followed a procedure similar to that for complex 1, except that *t*BuOXD- BF_3K replaced OXD- SO_3Na . $^1\text{H-NMR}$ (500 MHz, $\text{DMSO-}d_6$, δ [ppm]): 9.31 (s, 1H), 8.53 (d, $J = 8.4$ Hz, 1H), 8.33 (t, $J = 7.9$ Hz, 1H), 8.27 (d, $J = 7.7$ Hz, 2H), 8.08 (s, 1H), 8.04 (d, $J = 7.8$ Hz, 2H), 7.97 (t, $J = 7.6$ Hz, 2H), 7.93–7.85

(m, 2H), 7.82 (d, $J = 7.6$ Hz, 1H), 7.77 (d, $J = 5.7$ Hz, 1H), 7.72 (d, $J = 5.7$ Hz, 1H), 7.68–7.62 (m, 3H), 7.58 (d, $J = 7.1$ Hz, 1H), 7.54 (t, $J = 6.4$ Hz, 1H), 7.35 (t, $J = 7.4$ Hz, 1H), 7.29 (s, 1H), 7.23 (t, $J = 7.0$ Hz, 1H), 7.20 (t, $J = 7.0$ Hz, 1H), 7.05–6.95 (m, 2H), 6.93–6.82 (m, 3H), 6.19 (t, $J = 8.0$ Hz, 2H), 1.34 (s, 9H). ^{13}C -NMR (126 MHz, $\text{DMSO}-d_6$, δ [ppm]): 166.75, 166.62, 165.03, 163.49, 154.63, 149.11, 149.04, 148.99, 148.62, 148.09, 146.01, 144.01, 143.96, 143.17, 141.65, 138.82, 138.69, 135.10, 132.65, 131.20, 131.03, 130.06, 129.63, 129.50, 127.11, 126.32, 126.14, 125.21, 124.97, 124.62, 123.82, 123.69, 123.52, 122.27, 122.05, 121.22, 120.82, 119.88, 119.83, 113.46, 111.45, 34.72, 30.75. HRMS (ESI, m/z): 646.15607 $[\text{Ir}(\text{ppy})_2(\text{pzpy})]^+$ (calc. 646.15772); 345.13827 $[\text{tBuOXD-BF}_3]^-$ (calc. 345.13915). Anal. found: C, 57.95; H, 4.26; N, 9.79. Anal. calcd for $\text{C}_{48}\text{H}_{40}\text{BF}_3\text{IrN}_7\text{O}$: C, 58.18; H, 4.07; N, 9.89.

OLED fabrication and characterization

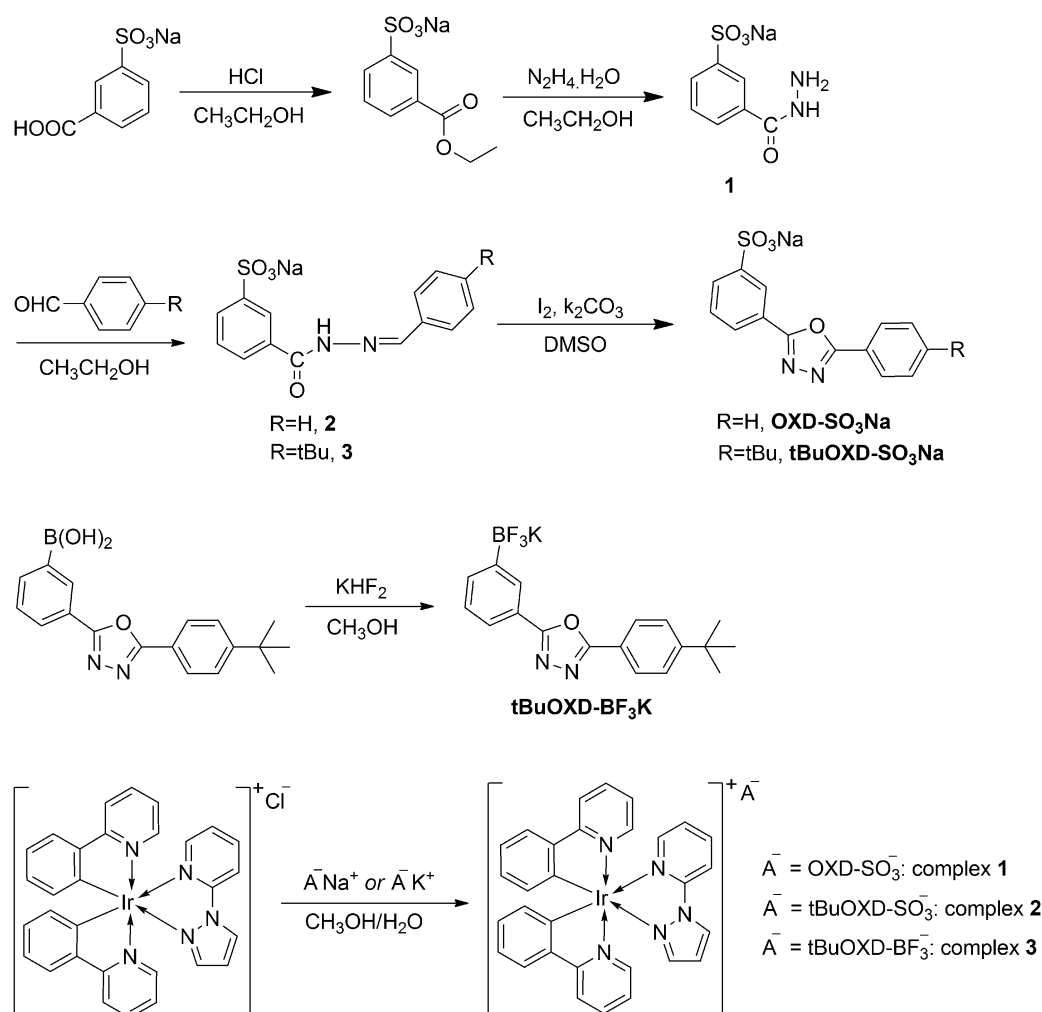
Indium-tin-oxide (ITO) coated glass substrates with a sheet resistance of $17 \Omega \square^{-1}$ were sufficiently cleaned in detergent and then in acetone and ethanol. Before use, the ITO substrates were exposed with UV-zone for 10 min. The PEDOT:PSS layer was spin-coated onto the ITO substrate and baked at 150°C

for 10 min. The emissive layer was then spin-coated on top of PEDOT:PSS from 1,2-dichloroethane solution (8 mg mL^{-1}) at 2000 rpm and baked at 80°C for 30 min in a nitrogen-filled glove box. The film-coated substrate was transferred into a high-vacuum chamber ($< 5 \times 10^{-4}$ Pa) and TmPyPB, LiF and Al layers were consecutively deposited by thermal evaporation at 1–2, 0.1 and 6 \AA s^{-1} , respectively. The devices were characterized in a nitrogen-filled glove box without exposure to air. The current density–voltage–brightness characteristics were measured by a Keithley 2400 source meter and a calibrated silicon photodiode. The EL spectra were recorded by an OPT-2000 fiber spectrometer.

3. Results and discussion

3.1. Synthesis and structural characterizations

Scheme 1 depicts the synthetic routes to the oxadiazole-type anions and complexes **1–3**. OXD- SO_3Na and $\text{tBuOXD-SO}_3\text{Na}$ can be readily prepared by starting from sodium 3-carboxybenzenesulfonate. Sodium 3-(hydrazinecarbonyl)benzenesulfonate (compound **1**) was conveniently prepared by esterification reaction of the starting compound, followed by hydrazinolysis of the ester.



Scheme 1 Synthetic routes to the oxadiazole-type anions and complexes **1–3**.

Sodium 3-(2-benzylidenehydrazine-1-carbonyl)benzenesulfonate (compounds **2**) and sodium 3-(2-(4-(*tert*-butyl)benzylidene)hydrazine-1-carbonyl)benzenesulfonate (compound **3**) were then prepared by condensation reaction of benzaldehyde or 4-*tert*-butyl benzaldehyde with compound **1**. OXD-SO₃Na and *t*BuOXD-SO₃Na were prepared with high yields (>80%) by iodine-assisted cyclization reactions of compounds **2** and **3**, respectively. *t*BuOXD-BF₃K was readily prepared from a boric ester precursor through a convenient -B(OR)₂ to -BF₃⁻ transformation in the presence of KHF₂. The complexes were prepared by anion-exchange reactions between [Ir(ppy)₂(pzpy)]⁺Cl⁻ and the oxadiazole-type anions in CH₃OH/H₂O solution. Chemical structures of the complexes were characterized by ¹H and ¹³C-NMR spectroscopies (Schemes S1–S6, ESI[†]), high-resolution mass spectrometry and elemental analysis.

3.2. Photophysical characterizations

Fig. 1 depicts the absorption and PL spectra of OXD-SO₃Na, *t*BuOXD-SO₃Na and *t*BuOXD-BF₃K in CH₃OH solution. The anions show strong absorption bands in the ultra-violet region below 325 nm, which should arise from the OXD core. From the absorption onset, the optical band gaps of OXD-SO₃⁻, *t*BuOXD-SO₃⁻ and *t*BuOXD-BF₃⁻ were estimated to be around 3.8 eV. In solution, OXD-SO₃Na, *t*BuOXD-SO₃Na and *t*BuOXD-BF₃K emit ultra-violet light peaked at 342, 349 and 337 nm, respectively. These emission bands overlap with the absorption of the [Ir(ppy)₂(pzpy)]⁺ cation (Fig. 2), which allows the occurrence of efficient Föster resonance energy transfer from the anions to [Ir(ppy)₂(pzpy)]⁺.

Fig. 2 shows the absorption and PL spectra of complexes **1–3** in CH₃CN solution. Detailed photophysical characteristics were summarized in Table 1. For comparison, those of the reference complex [Ir(ppy)₂(pzpy)]PF₆ (complex **R**) were also shown. The complexes show strong absorption bands below 350 nm, which should arise from the oxadiazole-type anions and the ligands in the [Ir(ppy)₂(pzpy)]⁺ cation. The complexes also show weak absorption bands above 350 nm that extends to the visible region, which are ascribed to the absorption of [Ir(ppy)₂(pzpy)]⁺, because similar weak absorption also appears in the absorption spectrum of complex **R** (Fig. 2).⁵⁰

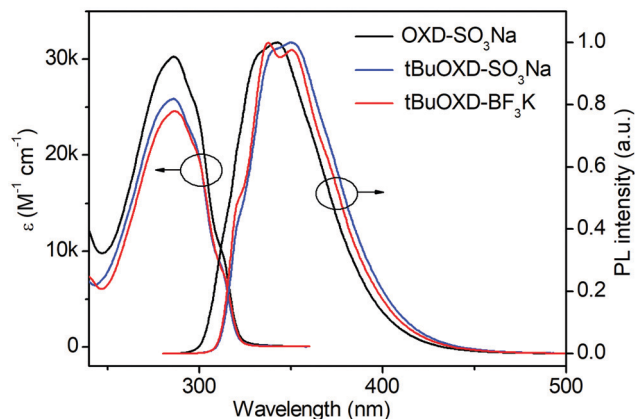


Fig. 1 Absorption and PL spectra of OXD-SO₃Na, *t*BuOXD-SO₃Na and *t*BuOXD-BF₃K in CH₃OH solution.

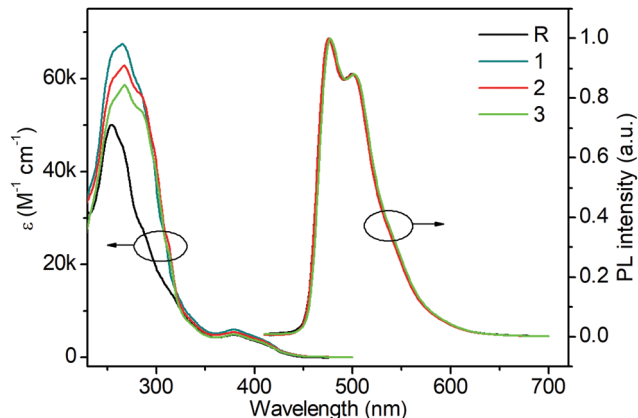


Fig. 2 Absorption and PL spectra of complexes **R** and **1–3** in CH₃CN solution. PL spectra were measured under excitation at 380 nm.

In degassed CH₃CN solution, complexes **1–3** afford blue-green emission peaked at around 475 and 500 nm under the excitation at 380 nm, which is almost the same as that afforded by complex **R** (Fig. 2).⁵⁰ Moreover, complexes **1–3** show very similar photoluminescent quantum yields (Φ) (0.21–0.22) and excited-state lifetimes (τ) (1.45–1.62 μ s) to complex **R** (Φ = 0.23 and τ = 1.56 μ s). From these Φ and τ values, the radiative and non-radiative decay rates of complexes **1–3** were calculated, which are also similar to those of complex **R** (Table 1). These experimental results reveal that the oxadiazole-type anions do not disturb the emission of the [Ir(ppy)₂(pzpy)]⁺ cation in solution. At excitation wavelengths shorter than 320 nm, both the oxadiazole-type anions and the [Ir(ppy)₂(pzpy)]⁺ cation are excited. At these excitation wavelengths, the complexes afford ultra-violet emission from the oxadiazole-type anions as well as blue-green emission from the [Ir(ppy)₂(pzpy)]⁺ cation (Fig. S1, ESI[†]), which indicates an incomplete energy-transfer from the oxadiazole-type anions to the [Ir(ppy)₂(pzpy)]⁺ cation in the solution. In solution, the counter-anion and the [Ir(ppy)₂(pzpy)]⁺ cation are not always in close proximity because of the fluid nature of the medium. For this reason, the energy transfer between them is inefficient in solution.

In the 2 wt% doped poly(methylmethacrylate) (PMMA) films, complexes **1–3** also afford blue-green emission peaked at around 475 and 505 nm under excitation at 380 nm, which resembles that from complex **R**. The complexes afford almost the same Φ (0.78–0.79) and τ (3.14–3.20 μ s) values as those of complex **R** (Φ = 0.80 and τ = 3.2 μ s), which further reveals that the oxadiazole-type anions do not affect the emission of the [Ir(ppy)₂(pzpy)]⁺ cation. In the thin films, the similar Φ and τ values for complexes **1–3** and complex **R** indicate that back triplet energy-transfer from the oxadiazole-type anions to [Ir(ppy)₂(pzpy)]⁺ does not occur owing to the high triplet energy (2.7 eV) of the OXD core. At excitation wavelengths shorter than 320 nm, both [Ir(ppy)₂(pzpy)]⁺ and oxadiazole-type anions are excited but complexes **1–3** show predominant blue-green emission from the [Ir(ppy)₂(pzpy)]⁺ cation and nearly no emission from the oxadiazole-type anions (Fig. S2, ESI[†]), which indicates an almost complete energy-transfer from the oxadiazole-type

Table 1 Photophysical data of complexes **1–3** in solution and doped films. For comparison, those of $[\text{Ir}(\text{ppy})_2(\text{pzpy})]\text{PF}_6$ (complex **R**) were also listed.^{31,50}

	Absorption λ [nm] (ϵ [$\times 10^4 \text{ M}^{-1} \text{ cm}^{-1}$]) ^a	PL in CH_3CN ^b					PL in PMMA film ^c				
		λ [nm]	Φ_p	τ [μs]	k_r, k_{nr} [10^5 s^{-1}]		λ [nm]	Φ_p	τ [μs]	k_r, k_{nr} [10^5 s^{-1}]	
1	266 (6.90), 380 (0.60), 408 (0.39)	475, 500	0.21	1.62	1.3, 4.9		475, 504	0.79	3.14	2.5, 0.7	
2	268 (6.27), 380 (0.54), 408 (0.34)	475, 500	0.21	1.45	1.4, 5.5		475, 505	0.78	3.17	2.5, 0.7	
3	268 (5.86), 380 (0.49), 408 (0.32)	477, 502	0.22	1.47	1.5, 5.3		475, 505	0.79	3.20	2.5, 0.7	
R	255 (5.00), 380 (0.48), 408 (0.30)	475, 503	0.23	1.56	1.5, 5.0		474, 502	0.80	3.20	2.5, 0.6	

^a In CH_3CN solution (10^{-5} M). ϵ denotes the molar extinction coefficient. ^b In degassed CH_3CN (10^{-5} M) solution. ^c In 2 wt% doped PMMA films.

anions to $[\text{Ir}(\text{ppy})_2(\text{pzpy})]^+$ in the PMMA films. The efficient energy-transfer in the highly diluted films reveals that the oxadiazole-type anion and the $[\text{Ir}(\text{ppy})_2(\text{pzpy})]^+$ cation are in close proximity in films because of the strong electrostatic interaction between them, which benefits the use of the complexes in thin-film light-emitting devices.

3.3. Electrochemical measurements

The electrochemical properties of the oxadiazole-type anions and complexes **R** and **1–3** were investigated through cyclic

voltammetry in solution. Fig. 3 shows the Cyclic voltammograms. In the solution, OXD- SO_3Na , *t*BuOXD- SO_3Na and *t*BuOXD- BF_3K all exhibit reversible reduction processes (Fig. 3a), which occur on the OXD core of the oxadiazole-type anions. The reversible reductions indicate that the oxadiazole-type anions have good stability for acceptance of electrons, which agrees with the electron-trapping/transporting property of the OXD core.^{47,48}

As shown in Fig. 3b, complexes **1–3** exhibit irreversible oxidation processes, which resemble the oxidation of complex **R**, indicating that the oxidations of complexes **1–3** occur on the $[\text{Ir}(\text{ppy})_2(\text{pzpy})]^+$ cation. In the solution, complexes **1–3** show two reduction processes, with the first one being irreversible and the second one being quasi-reversible. These two reduction processes should result from the reductions of $[\text{Ir}(\text{ppy})_2(\text{pzpy})]^+$ cation and oxadiazole-type anion, respectively, because similar reduction processes appear in the cyclic voltammograms of complex **R** and oxadiazole-type anions (Fig. 3a and b).

3.4. Solution-processed OLEDs

Complexes **1–3** were tested as dopants in solution-processed OLEDs with a structure of ITO/PEDOT:PSS (40 nm)/26DCzPPy: *x*% complex (50 nm)/TmPyPB (40 nm)/LiF (1 nm)/Al (100 nm), where 2,6-bis(3-(carbazol-9-yl)phenyl)pyridine (26DCzPPy) was used as the host and 1,3,5-tri[(3-pyridyl)-phen-3-yl]benzene (TmPyPB) was used as the electron-transporting/hole-blocking layer. For comparison, the device using complex **R** as a dopant was also fabricated. The emissive layers were deposited by solution-processes. The doping concentrations of complexes **1–3** and **R** in the emissive layers were set at 12 wt%, 12 wt%, 12 wt% and 10 wt%, respectively, so that the doping concentrations of $[\text{Ir}(\text{ppy})_2(\text{pzpy})]^+$ were all at 8 wt%.

Fig. 4 depicts the EL spectra of the OLEDs. The devices all showed blue-green EL peaked at around 480 and 510 nm, with Commission Internationale de L'Eclairage (CIE) coordinates at around (0.18, 0.49). The nearly identical EL spectra indicate that the emission of all devices arose from the $[\text{Ir}(\text{ppy})_2(\text{pzpy})]^+$ cation. The PL spectra of the emissive layers show dominant emission from $[\text{Ir}(\text{ppy})_2(\text{pzpy})]^+$ (Fig. S3, ESI[†]), which indicates efficient energy-transfer from the 26DCzPPy host and the oxadiazole-type anions to $[\text{Ir}(\text{ppy})_2(\text{pzpy})]^+$ in the emissive layers.

Fig. 5 shows the current density–voltage–brightness curves of the OLEDs. Detailed device performances were summarized in Table 2. As shown in Fig. 5, the devices using complexes **1–3** as dopants all showed lower current-density than the device using complex **R** as the dopant. From the energy level diagrams of the devices (Scheme S7, ESI[†]), the oxadiazole-type anions are

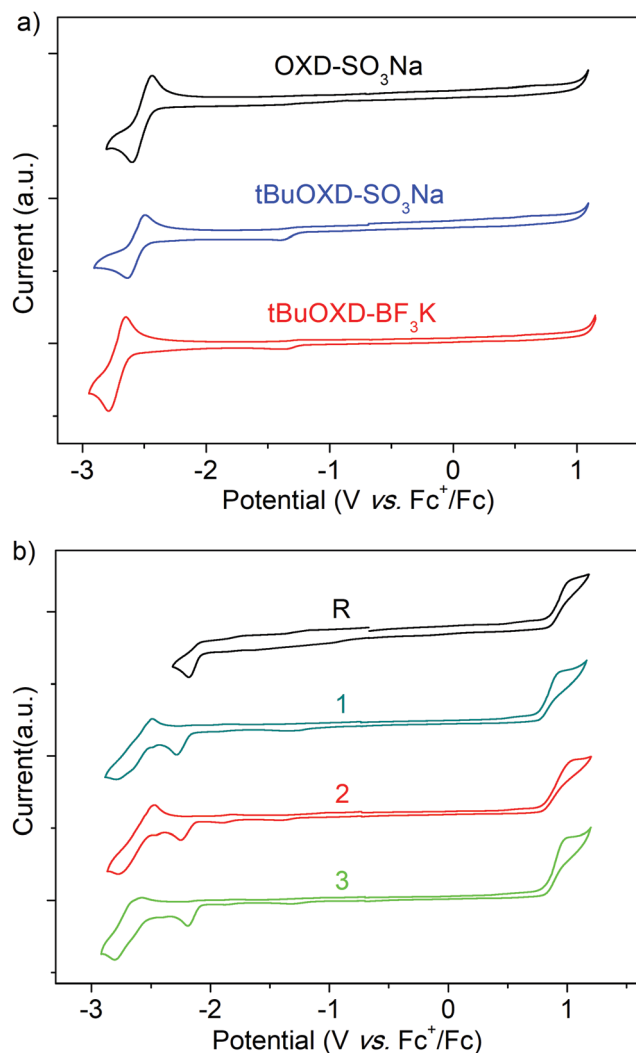


Fig. 3 Cyclic voltammograms of (a) oxadiazole-type anions and (b) complexes **R** and **1–3** in DMF solution.

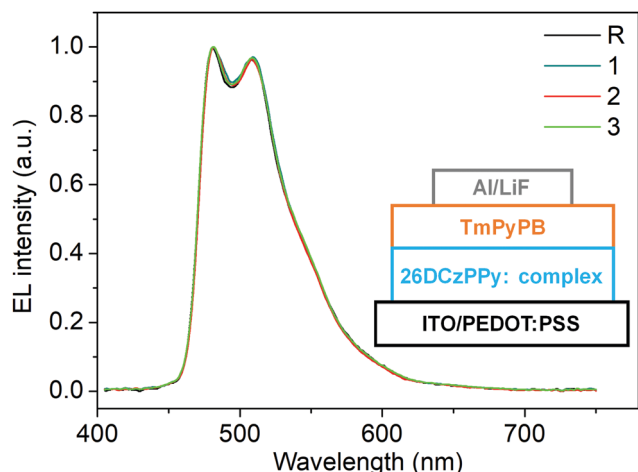


Fig. 4 EL spectra of OLED devices using complexes **R** and **1–3**. Inset shows the device structure.

found to behave as electron-traps in the emissive layers when they cannot form electron-transporting channels within the layers at low doping concentrations (4 wt%).⁵¹ The lowered current density for the devices using complexes **1–3** agrees with the electron-trapping effects of the oxadiazole-type counter-anions in the emissive layers.^{51–53}

As shown in Table 2, the reference device using complex **R** afforded a peak current efficiency and a peak EQE of 26.6 cd A^{-1} and 10.2%, respectively. For comparison, the devices using complexes **1–3** showed much higher performances, with peak current efficiencies of 37.6, 33.8 and 33.1 cd A^{-1} , respectively, and peak EQEs of 15.2%, 13.6% and 13.2%, respectively. The largely enhanced device performances reveal the advantages of using oxadiazole-type counter-anions for the use of cationic iridium complexes in light-emitting devices. The electron-trapping on the oxadiazole-type anions would on one hand achieve better hole/electron-transport balance in the emissive layers, and on the other hand, facilitate direct carrier recombination on the $[\text{Ir}(\text{ppy})_2(\text{pzpy})]^+$ cation because of the close proximity between the counter-anion and the $[\text{Ir}(\text{ppy})_2(\text{pzpy})]^+$ cation. These effects help to improve

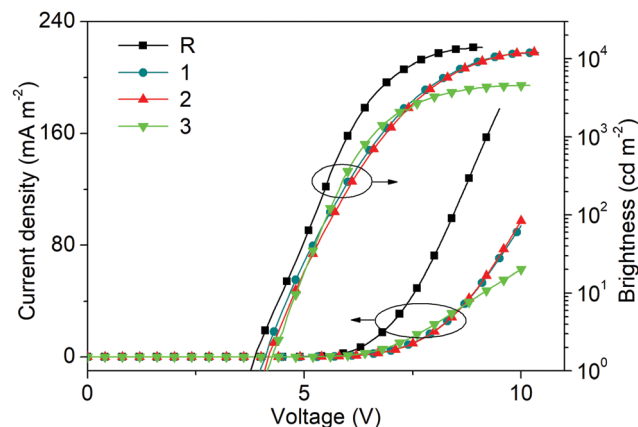


Fig. 5 Current-density and brightness versus voltage curves for OLED devices using complexes **R** and **1–3**.

Table 2 Summary of performances for OLED devices using complexes **R** and **1–3**

Complex	V_{on}^a (V)	$\eta_{\text{c,max}}^b$ (cd A^{-1})	$\text{EQE}_{\text{max}}^c$ (%)	B_{max}^d (cd m^{-2})	EL λ (nm)	CIE (x, y)
R	3.8	26.6	10.2	14 000	480, 509	(0.19, 0.49)
1	4.0	37.6	15.2	12 000	481, 510	(0.18, 0.49)
2	4.1	33.8	13.6	12 000	480, 509	(0.18, 0.49)
3	4.1	33.1	13.3	4600	480, 509	(0.18, 0.49)

^a Voltage to reach 1 cd m^{-2} . ^b Maximum current efficiency. ^c Maximum external quantum efficiency. ^d Maximum brightness.

the carrier-recombination balance and thus the performances of the devices. Similar electron-trapping effects that promote carrier recombination balance have been observed in OLEDs using neutral iridium complexes with electron-trapping oxadiazole or triazole-type units.^{52–54} In addition, the Φ values of the emissive layers for devices using complexes **R** and **1–3** were measured to be 0.66, 0.72, 0.71 and 0.70, respectively. The higher Φ values for complexes **1–3** compared to complex **R** in the emissive layers could be related to suppression of inter-complex interactions caused by the bulky counter-anions in complexes **1–3**.³⁶ By assuming a light out-coupling efficiency of 0.2, the theoretical EQE for the device using complex **R** was estimated to be 13.2%, which is considerably higher than the experimental one (10.2%), indicating an unbalanced carrier recombination in the device using complex **R**. The theoretical EQEs of the devices using complexes **1–3** were estimated to be 14.0–14.4%, which agree with the experimental ones (13.3–15.2%), indicating nearly balanced carrier-recombination in the devices using complexes **1–3**. It is thus concluded that the enhanced device performances for cationic iridium complexes using oxadiazole-type counter-anions can be ascribed to improved carrier-recombination balance (major effect) and enhanced Φ values (minor effect) in the emissive layer.

It is worth noting that the efficiency afforded by the device using complex **1** (EQE = 15.2%) is the highest for solution-processed OLEDs using cationic iridium complexes reported so far (Table S1, ESI†).^{13–32} This efficiency is higher than that (9.8%) afforded by the multilayer vacuum-evaporation blue-green OLEDs using the $[\text{Ir}(\text{ppy})_2(\text{pzpy})]^+$ cation,⁵⁵ and even comparable to the highest one (16.4% for a green-yellow device) for multilayer vacuum-evaporation OLEDs using cationic iridium complexes (Table S1, ESI†).⁴⁰ It is noted that $[\text{Ir}(\text{ppy})_2(\text{pzpy})]^+$ is not the most efficient blue-green phosphorescent cation.^{31,44} Even higher device performances can be expected by using more efficient phosphorescent cations in combination with the oxadiazole-type counter-anions.

As shown in Table 2, devices using complexes **1–3** show slightly higher turn-on voltages than the device using complex **R**, which agrees with the electron-trapping effect of the oxadiazole-type anions in complexes **1–3**.⁵¹ The device using complex **2** showed lower efficiencies than the device using complex **1**, which suggests that the bulky *tert*-butyl group in *t*BuOXD- SO_3^- could hinder the carrier-transport/recombination in the emissive layer. The device using complex **3** showed comparable high efficiencies to the devices using complexes **1** and **2** but much lower maximum brightness, which suggests that the phenyltrifluoroborate anion

in $t\text{BuOXD-BF}_3^-$ has lower stability than the benzenesulfonate anion in OXD-SO_3^- or $t\text{BuOXD-SO}_3^-$ in operating OLEDs, presumably due to the low chemical stability of B-C(sp²) bonds.⁵⁶ All devices showed decreased current efficiencies and EQEs at high brightness (Fig. S4, ESI[†]), owing to the triplet-triplet or triplet-polaron quenching at high current densities.^{57,58} Nevertheless, the devices using complexes 1 and 2 still showed high current efficiencies of 35.7 and 32.5 cd A⁻¹, respectively, at 1000 cd m⁻², which indicates widened carrier recombination zones in the emissive layers.

4. Conclusion

A series of oxadiazole-type counter-anions, OXD-SO_3^- , $t\text{BuOXD-SO}_3^-$ and $t\text{BuOXD-BF}_3^-$, and blue-green-emitting cationic iridium complexes using them have been prepared and characterized. These counter-anions affect neither the emission nor the electrochemical properties of the phosphorescent iridium cation. In films, the anion and the phosphorescent cation are closely bound together which allows efficient energy-transfer between them. The new complexes showed remarkably enhanced performances compared to the reference complex with a PF_6^- counter-anion in solution-processed OLEDs, with a record-high external quantum efficiency of 15.2% from a double-layer structure. Even higher device performances can be expected by combining these oxadiazole-type anions with more efficient phosphorescent cations. The work has revealed that cationic iridium complexes with oxadiazole-type counter-anions can achieve performances comparable to neutral complexes in solution-processed OLEDs, which afford highly efficient devices with a great potential for display or lighting applications.

Conflicts of interest

There are no conflicts to declare.

Acknowledgements

We thank the National Natural Science Foundation of China (Grant No. 51773074), the program of introducing talents of discipline to universities of china (111 program, B17019), and the self-determined research funds of CCNU from the colleges' basic research and operation of MOE for financial support.

References

- 1 C. W. Tang and S. A. VanSlyke, *Appl. Phys. Lett.*, 1987, **51**, 913–915.
- 2 N. T. Kalyani, H. Swart and S. J. Dhoble, *Principles and Applications of Organic Light Emitting Diodes (OLEDs)*, Woodhead Publishing, 2017.
- 3 R. Abbel, Y. Galagan and P. Groen, *Adv. Eng. Mater.*, 2018, **20**, 1701190.
- 4 C. M. Zhong, C. H. Duan, F. Huang, H. B. Wu and Y. Cao, *Chem. Mater.*, 2011, **23**, 326–340.
- 5 K. S. Yook and J. Y. Lee, *Adv. Mater.*, 2014, **26**, 4218–4233.
- 6 T. Chiba, Y. J. Pu and J. Kido, *J. Mater. Chem. C*, 2015, **3**, 11567–11576.
- 7 S. H. Ho, S. Y. Liu, Y. Chen and F. So, *J. Photon. Energy*, 2015, **5**, 057611.
- 8 J. F. Liang, L. Ying, F. Huang and Y. Cao, *J. Mater. Chem. C*, 2016, **4**, 10993–11006.
- 9 T. Y. Huang, W. Jiang and L. Duan, *J. Mater. Chem. C*, 2018, **6**, 5577–5596.
- 10 Y. Zou, S. L. Gong, G. H. Xie and C. L. Yang, *Adv. Opt. Mater.*, 2018, **6**, 1800568.
- 11 S. Jhulki, M. W. Cooper, S. Barlow and S. R. Marder, *Mater. Chem. Front.*, 2019, **3**, 1699–1721.
- 12 D. Ma, T. Tsuboi, Y. Qiu and L. Duan, *Adv. Mater.*, 2017, **29**, 1603253.
- 13 E. A. Plummer, A. van Dijken, H. W. Hofstraat, L. De Cola and K. Brunner, *Adv. Funct. Mater.*, 2005, **15**, 281–289.
- 14 L. He, L. Duan, J. Qiao, D. Q. Zhang, G. F. Dong, L. D. Wang and Y. Qiu, *Org. Electron.*, 2009, **10**, 152–157.
- 15 L. He, L. Duan, J. Qiao, D. Q. Zhang, L. D. Wang and Y. Qiu, *Org. Electron.*, 2010, **11**, 1185–1191.
- 16 L. He, L. A. Duan, J. A. Qiao, D. Q. Zhang, L. D. Wang and Y. Qiu, *Appl. Phys. A: Mater. Sci. Process.*, 2010, **100**, 1035–1040.
- 17 J. M. Fernandez-Hernandez, C. H. Yang, J. I. Beltran, V. Lemaure, F. Polo, R. Frohlich, J. Cornil and L. De Cola, *J. Am. Chem. Soc.*, 2011, **133**, 10543–10558.
- 18 H. J. Tang, Y. H. Li, B. F. Zhao, W. Yang, H. B. Wu and Y. Cao, *Org. Electron.*, 2012, **13**, 3211–3219.
- 19 R. Tao, J. Qiao, G. L. Zhang, L. Duan, L. D. Wang and Y. Qiu, *J. Phys. Chem. C*, 2012, **116**, 11658–11664.
- 20 L. He, L. Duan, J. Qiao, D. Q. Zhang, G. F. Dong, L. D. Wang and Y. Qiu, *Synth. Met.*, 2013, **166**, 52–56.
- 21 H. J. Tang, Y. H. Li, Q. L. Chen, B. Chen, Q. Q. Qiao, W. Yang, H. B. Wu and Y. Cao, *Dyes Pigm.*, 2014, **100**, 79–86.
- 22 H. J. Tang, L. Y. Wei, G. Y. Meng, Y. H. Li, G. Z. Wang, F. R. Yang, H. B. Wu, W. Yang and Y. Cao, *Opt. Mater.*, 2014, **37**, 679–687.
- 23 F. L. Zhang, D. X. Ma, L. Duan, J. Qiao, G. F. Dong, L. D. Wang and Y. Qiu, *Inorg. Chem.*, 2014, **53**, 6596–6606.
- 24 D. X. Ma, L. Duan and Y. Qiu, *Dalton Trans.*, 2015, **44**, 8521–8528.
- 25 H. J. Tang, Z. Y. Chen, L. Y. Wei, J. S. Miao, G. Y. Meng, Y. H. He and H. B. Wu, *Dyes Pigm.*, 2016, **131**, 340–348.
- 26 D. X. Ma, C. Zhang, Y. Qiu and L. Duan, *J. Mater. Chem. C*, 2016, **4**, 5731–5738.
- 27 N. Z. Luo, Y. Lan, R. R. Tang, L. He and L. Duan, *Chem. Commun.*, 2016, **52**, 14466–14469.
- 28 A. F. Henwood, A. K. Bansal, D. B. Cordes, A. M. Z. Slawin, I. D. W. Samuel and E. Zysman-Colman, *J. Mater. Chem. C*, 2016, **4**, 3726–3737.
- 29 F. L. Zhang, C. F. Si, D. H. Wei, S. S. Wang, D. P. Zhang, S. Z. Li, Z. Y. Li, F. Q. Zhang, B. Wei, G. X. Cao and B. Zhai, *Dyes Pigm.*, 2016, **134**, 465–471.
- 30 M. T. Sajjad, N. Sharma, A. K. Pal, K. Hasan, G. Xie, L. S. Kölln, G. S. Hanan, I. D. W. Samuel and E. Zysman-Colman, *J. Mater. Chem. C*, 2016, **4**, 8939–8946.

- 31 L. He, Y. Lan, D. X. Ma, X. Z. Song and L. Duan, *J. Mater. Chem. C*, 2018, **6**, 1509–1520.
- 32 P. Wang, N. Z. Luo, X. Z. Song and L. He, *ChemPlusChem*, 2018, **83**, 246–253.
- 33 X. W. Meng, R. B. Bai, X. X. Wang, F. F. Pan and L. He, *Dyes Pigm.*, 2019, **165**, 458–466.
- 34 K. A. King and R. J. Watts, *J. Am. Chem. Soc.*, 1987, **109**, 1589–1590.
- 35 R. B. Bai, X. W. Meng, X. X. Wang and L. He, *Adv. Funct. Mater.*, 2020, DOI: 10.1002/adfm.201907169.
- 36 D. X. Ma, L. Duan, Y. G. Wei, L. He, L. D. Wang and Y. Qiu, *Chem. Commun.*, 2014, **50**, 530–532.
- 37 S. Tang and L. Edman, *Top. Curr. Chem.*, 2016, **374**, 40.
- 38 D. X. Ma, Y. Qiu and L. Duan, *Adv. Funct. Mater.*, 2016, **26**, 3438–3445.
- 39 D. X. Ma, L. Duan and Y. Qiu, *J. Mater. Chem. C*, 2016, **4**, 5051–5058.
- 40 D. Ma, C. Zhang, R. Liu, Y. Qu and L. Duan, *ACS Appl. Mater. Interfaces*, 2018, **10**, 29814–29823.
- 41 D. X. Ma and L. Duan, *Chem. Rec.*, 2019, **19**, 1483–1498.
- 42 C. Zhang, D. X. Ma, R. H. Liu and L. Duan, *J. Mater. Chem. C*, 2019, **7**, 3503–3511.
- 43 L. Ding, C. X. Zang, H. T. Mao, G. G. Shan, L. L. Wen, H. Z. Sun, W. F. Xie and Z. M. Su, *Chem. Commun.*, 2018, **54**, 11761–11764.
- 44 M. Z. Chen, S. R. Wang, X. Z. Song and L. He, *J. Phys. Chem. C*, 2018, **122**, 28256–28264.
- 45 C. Wu, H. F. Chen, K. T. Wong and M. E. Thompson, *J. Am. Chem. Soc.*, 2010, **132**, 3133–3139.
- 46 M. Mauro, K. C. Schuermann, R. Pretot, A. Hafner, P. Mercandelli, A. Sironi and L. D. Cola, *Angew. Chem., Int. Ed.*, 2010, **49**, 1222–1226.
- 47 A. P. Kulkarni, C. J. Tonzola, A. Babel and S. A. Jenekhe, *Chem. Mater.*, 2004, **16**, 4556–4573.
- 48 G. Hughes and M. R. Bryce, *J. Mater. Chem.*, 2005, **15**, 94–107.
- 49 J. Zhang, L. Zhou, H. A. Al-Attar, K. Shao, L. Wang, D. Zhu, Z. Su, M. R. Bryce and A. P. Monkman, *Adv. Funct. Mater.*, 2013, **23**, 4667–4677.
- 50 L. He, L. Duan, J. Qiao, R. J. Wang, P. Wei, L. D. Wang and Y. Qiu, *Adv. Funct. Mater.*, 2008, **18**, 2123–2131.
- 51 X. Gong, J. C. Ostrowski, D. Moses, G. C. Bazan and A. J. Heeger, *Adv. Funct. Mater.*, 2003, **13**, 439–444.
- 52 H. Y. Li, T. Y. Li, M. Y. Teng, Q. L. Xu, S. Zhang, Y. M. Jin, X. Liu, Y. X. Zheng and J. L. Zuo, *J. Mater. Chem. C*, 2014, **2**, 1116–1124.
- 53 G. Z. Lu, L. Liu, Z. L. Tu, Y. H. Zhou and Y. X. Zheng, *J. Mater. Chem. C*, 2019, **7**, 2022–2028.
- 54 T. Giridhar, C. Saravanan, W. Cho, Y. G. Park, J. Y. Lee and S. H. Jin, *Chem. Commun.*, 2014, **50**, 4000–4002.
- 55 D. X. Ma, Y. Qiu and L. Duan, *ChemPlusChem*, 2018, **83**, 211–216.
- 56 D. T. Yang, S. K. Møllerup, J. B. Peng, X. Wang, Q. S. Li and S. N. Wang, *J. Am. Chem. Soc.*, 2016, **138**, 11513–11516.
- 57 W. Staroske, M. Pfeiffer, K. Leo and M. Hoffmann, *Phys. Rev. Lett.*, 2007, **98**, 197402.
- 58 S. Reineke, K. Walzer and K. Leo, *Phys. Rev. B: Condens. Matter Mater. Phys.*, 2007, **75**, 125328.